AIAA JOURNAL
Vol. 49, No. 8, August 2011

# Understanding How Chevrons Modify Noise in a Supersonic Jet with Flight Effects

O. Rask,* J. Kastner,† and E. Gutmark‡
*University of Cincinnati, Cincinnati, Ohio 45221*

DOI: 10.2514/1.J050628

**Tests were conducted to determine the effect of chevrons on the sound radiated from the exhaust of a Mach 1.19 core flow with simulated flight effects. Flight effects were studied by using a secondary coaxial flow varied from static to Mach 0.50. Shadowgraphy, static pressure, and turbulence measurements were used to complement near-field pressure and far-field acoustic measurements. The presence of a secondary flow causes the shock-cell length to slightly lengthen and the shock cells to persist farther downstream; this was true for both the baseline and chevron nozzles. Compared with the baseline nozzle, the shadowgraphy and near-field static pressure showed that the chevrons reduced the shock-cell spacing with minimal effect on the shock-cell strength. Higher turbulence levels near the nozzle exit and comparable shock-cell strength led to higher shock-associated noise for the chevron configuration compared with the baseline. The decrease in shock-cell length caused the peak amplitude of the shock-associated noise to shift to higher frequencies. At the same time, the chevrons significantly reduced any screech tones that were initially present for the baseline case. Finally, it was shown that the chevrons reduced turbulence levels near the end of the potential core, which resulted in a reduction of the low-frequency mixing noise that dominates the aft angles.**

## Nomenclature

| | | |
|---|---|---|
| $D_{eq}$ | = | equivalent diameter |
| $M_j$ | = | jet Mach number |
| $M_1$ | = | primary jet Mach number |
| $M_2$ | = | secondary jet Mach number |
| $L$ | = | shock-cell length |
| $P$ | = | pressure |
| $P_0$ | = | total pressure |
| $R$ | = | radial coordinate |
| $u$ | = | axial fluctuating velocity |
| $V_{exit}$ | = | velocity at nozzle exit |
| $v$ | = | radial fluctuating velocity |
| $X$ | = | axial coordinate |
| $\langle\,\rangle$ | = | ensemble average |

## I. Introduction

CHEVRONS have been studied for years as a means of reducing mixing noise created by subsonic discharge velocities [1–7]. Recently, they have started appearing on production engines [8]. This is beneficial for community noise issues during takeoff and landing cycles, when flight speeds are relatively low. However, when an airplane if flying at cruise conditions, the flow discharging from the engines is supersonic. Advances in mixing-noise reduction have been successful enough that shock noise is now emerging as a dominant source during cruise. Shock noise is of primary concern to the crew and passengers of commercial aircraft. It can be mitigated by adding weight, in the form of acoustically absorbent materials, to the hull of an airplane. However, it would be preferable to reduce shock noise at the source. Chevrons have been shown to be effective at reducing mixing noise for subsonic conditions. It would be ideal if they could also be used to mitigate shock noise at supersonic conditions.

Shock noise is created as turbulence interacts with shock cells in a nonideally expanded jet [9]. Shock noise created by an individual cell interacts constructively/destructively with adjacent cells. This results in preferred frequencies, depending on observer angle. At 90 deg to the flow, the peak/center frequency of shock noise is directly proportional to the convective velocity and indirectly proportional to the shock-cell spacing. The center frequency of shock noise is lower at forward angles and higher at the aft angles [10]. Additionally, shock noise is louder than mixing noise at forward angles, and at aft angles the opposite is true. Experimental investigations discharging into quiescent mediums have confirmed this. Experimental investigations of supersonic flows discharging with a surrounding secondary flow, or coflow, have also been performed. The additional stream reduces mixing, lengthens the potential core, and increases the number of shock cells and their spacing [11,12]. In accordance with theory, the resulting shock-associated noise has a lower center/peak frequency.

Chevrons that are immersed in a high-speed flow create counter-rotating streamwise vortices. The vortices accelerate mixing between the two streams and are effective at reducing low-frequency mixing noise. However, the vortices also introduce additional turbulence, one of the required components of shock noise. The amount of additional turbulence is a function of how much the chevrons penetrate and the shear velocity between the two streams. Simply put, the more the chevrons penetrate and the higher the shear velocity, the more turbulence is generated. For noise-reduction applications, the increased turbulence often leads to a high-frequency noise penalty. Chevrons thus have limited penetration in commercial aircraft application to avoid such a penalty. The reduced penetration also has the benefit of having less thrust loss.

Samimy et al. [13] demonstrated that tabs effectively reduce the strength of shock cells. The results for chevrons are not as clear. Using a wind tunnel, Long [14,15] demonstrated that chevrons can either increase or decrease the magnitude of shock noise, but did not explain the mechanism. Mengle et al. [16] demonstrated that chevrons have a beneficial effect on shock noise when installed on a full-scale engine and tested in flight. Bultemeier et al. [17] demonstrated the effect on cabin noise for chevrons with various penetrations. Chevrons with minimal penetration resulted in significant noise reduction and as the penetration of the chevron increased the low-frequency noise benefit began to be accompanied with a high-frequency penalty. However, both papers did not examine the flow physics in any detail. This work investigates both the flowfield and far field of baseline and chevron nozzle configurations to understand

Received 26 April 2010; revision received 7 March 2011; accepted for publication 17 March 2011. 

*Department of Aerospace Engineering and Engineering Mechanics; currently General Electric; olaf.rask@ge.com. Member AIAA.

†Research Professor, Department of Aerospace Engineering and Engineering Mechanics; kastnejy@ucmail.uc.edu. Member AIAA.

‡Distinguished Professor, Department of Aerospace Engineering and Engineering Mechanics, Department of Otolaryngology—Head and Neck Surgery; gutmarej@ucmail.uc.edu. Fellow AIAA.

how the shock-cell strength and length are affected by the chevrons and then to understand how these changes affect the screech, shock-associated noise, and mixing noise. At the same time, the effect of forward flight is investigated, since the problem being addressed is during cruise, when flight effects are significant.

## II. Experimental Setup

All tests were conducted in the Acoustic Test Facility (ATF) at the University of Cincinnati, which contains a $24 \times 25 \times 11$ ft anechoic chamber. The chamber is acoustically treated to provide a lower cutoff frequency of 400 Hz. A complete description of the ATF and associated instrumentation is available in Callender et al. [18]. The ATF does not have the capability to accurately simulate flight effects. For this reason, the core flow was used to simulate the total discharge of a bypass engine, and the fan flow was used to simulate the flight condition. In Fig. 1, the two streams are shown. The core nozzle was converging only and discharged a 5.2 cm equivalent-diameter $D_{eq}$ underexpanded jet at a jet Mach number of 1.19 surrounded by a 10.3 cm equivalent-diameter coaxial flow. The normalized pressure ratio (NPR) was 2.39, the exit velocity $V_{exit}$ was 364 m/s, and the stagnation temperature was 300 K. The core stream had a Reynolds number based on the jet diameter of $2 \times 10^6$. The fan stream had a stagnation temperature of 300 K and was set to discharge at one of three Mach numbers ($M_2$) of 0.00, 0.28, and 0.50, which corresponded to NPRs of 0.0, 1.056, and 1.186, respectively. A baseline and an eight-chevron low-penetration ($\sim$1% of jet radius) nozzle were used on the core stream, while only an axisymmetric nozzle was used on the fan stream. The boundary layer at the core nozzle exit was not measured for the current conditions, but for near-sonic conditions ($M_1 = 0.96$), it was found that the boundary layer was about double the core chevron's penetration. Thus, it is assumed for the current investigation that the chevron was completely immersed in the boundary layer.

Several comments concerning the validity of this experiment are required. In these tests, the primary flow simulated the total discharge (fan and core) of an engine. Therefore, the inner shear layer of an engine in flight was not represented in the experiment. Alternatively, the shear layer between secondary flow and the quiescent surroundings of the test chamber does not exist for an engine in flight. This redundant shear layer will modify shock noise as it passes through. The experiments comparing the chevrons to the baseline were valid if there was no difference between the outer shear layer created with the baseline nozzle and the outer shear layer created with the chevron nozzle. If the shear layers created by the baseline and chevron nozzles were largely identical, then shock noise was modified identically as it propagated through. However, if the chevron nozzle modified the outer shear layer, shock noise propagation was not the same and would make shock noise comparison tentative. To reduce this possibility, a low-penetration chevron nozzle was used for this study, which minimized any effect to the outer shear layer. In addition, because the fan stream did not have infinite thickness, it is possible that turbulence of the outer shear layer interacted with the shock cells, which would influence the results. Secondary Mach numbers up to 0.50 were studied, since this ensured that the turbulence levels between the outer shear layer and ambient were lower than the turbulence levels between the primary stream and the secondary stream.

A LaVision particle imagery velocimetry (PIV) system was used to measure the axial and radial velocity components along a streamwise laser sheet downstream of the centerbody tip. Illumination of the sheet is provided by a New Wave laser that emits 120 mJ/pulse at 532 nm. Laser optics form the laser beam into a thin two-dimensional sheet that passed through the jet centerline, and for the chevron case the sheet was aligned with the trough. Two-dimensional streamwise images were acquired at 5 Hz using two $1376 \times 1040$ 12-bit digital cameras mounted side by side. The flowfield was seeded using custom-designed olive oil atomizers, which have shown to provide particle seeds with a diameter on the order of 1 $\mu$m [4]. A total of 500 image pairs were acquired at each axial location. Since the acquisition was at 5 Hz, there is no time correlation between successive image pairs. The nozzle hardware was painted with antireflection fluorescent paint containing rhodamine dye. The dye shifted the reflected light to a different wavelength that was then filtered out by the 532 nm bandpass filters mounted to each camera. Images were processed using DaVis version 7.1 software using a multipass scheme. The results section presents radial turbulence profiles at $X/D_{eq} = 2.0$ and 8.0. Each radial profile contains 44 points spanning from the jet centerline ($R/D_{eq} = 0.00$) to $R/D_{eq} = 2.25$. This yields a vector spacing of $0.05D_{eq}$.

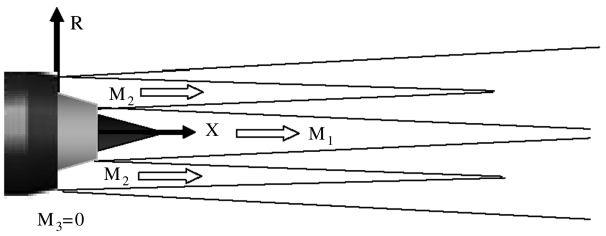


**Fig. 1 Schematic of dual-stream facility simulating forward-flight effects.**

The accuracy of the PIV measurements is limited by the ability of the olive oil particles to follow the motion of the flow. The tradeoff is based on the particle being large enough to ensure that laser light is scattered, but small enough to ensure that the particle can trace the flow and respond to higher frequencies [19]. The diameter of the particles is about 1 $\mu$m, which ensures a frequency response up to 10 kHz and an uncertainty in the turbulence intensity of about 5%. The microphones used for the near-field and far-field acoustic data are accurate beyond this frequency, but the peak amplitude in shock-associated noise was at around 10 kHz, which is in the range of the PIV capabilities. The repeatability of the measurements was found to be $\pm$5% at $X/D_{eq} = 2.0$ and $\pm$10% at $X/D_{eq} = 8.0$ for the downstream positions.

Point measurements of static pressure are performed using a supersonic five-hole conical probe (United Sensor model SDF-15-6-15-600). The sensor has a truncated cone with a half-angle of 15 deg, a total pressure port is located at the tip of the truncated cone, and four side ports are evenly spaced around the conic surface. Such a probe has a shock in front of it when submersed in supersonic flow, but the flowfield between this conic shock and the conic surface of the probe may be solved for, and the shock angle and upstream Mach number may be determined. The shock in the immediate vicinity of the probe tip is normal, and since the total pressure behind the shock is measured and the Mach number is known, the total and static pressure before the shock can be determined. When the side port pressure values are averaged, as was currently done, the Mach number result is insensitive to yaw angle changes up to 10 deg [20]. It was mounted on a computer-controlled traverse for testing and had a radial position of $0.1D_{eq}$ below the jet centerline. This was done to avoid any interference from the centerbody wake. A total of 55 points were taken from $X/D_{eq} = 1.58$ to 8.09, giving a spatial resolution of $0.18D_{eq}$.

Acoustic measurements are made with eight B&K condenser microphones, which have an uncertainty of $\pm$0.25 dB. The microphones can measure frequencies to a maximum 100 kHz. For far-field testing, they are placed on a $70D_{eq}$ (core equivalent diameters) radial arc with the origin at the centerbody tip and spanning polar arc angles from 70 to 150 deg relative to the relative to the forward-flight direction. For near-field testing the microphones were placed on a near-field linear array angled 10 deg relative to the jet axis beginning at nozzle exit and $2D_{eq}$ away from the jet centerline. The data were sampled at 204.8 kHz, and 500 blocks of 4096 points were acquired. The sound data were then postprocessed to provide both narrowband spectral data and overall sound pressure level (OASPL).

## III. Results

### A. Flowfield

Shadowgraphy was used to examine the initial development of the shear layer for the three secondary flows tested ($M_2 = 0.00$, 0.28, and 0.50) with and without chevrons on the primary nozzle. Results

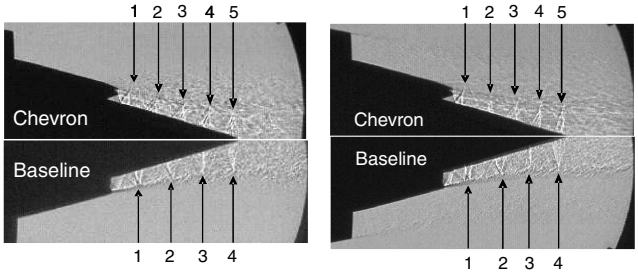


**Fig. 2 Shadowgraphs for baseline and chevron configurations, primary flow at a Mach number of 1.19 (fully expanded), secondary flow (left) at a Mach number of 0.00, and secondary flow (right) at a Mach number of 0.50.**

for the lowest and highest secondary Mach numbers are shown in Fig. 2. For all cycle conditions, four standing shock waves exist upstream of the centerbody tip for the baseline configuration, while there are five standing shock waves in the same region for the chevron configuration. Also, downstream of the centerbody tip, the shock cells are weaker for all secondary flows and both nozzle configurations.

Shown in Fig. 3 are normalized static pressure results along the jet plume centerline and downstream of the centerbody tip for both the baseline and chevron configurations. The first static pressure maximums coincided for all cases, which agrees with the shadowgraphy results that showed the shock cells in alignment on the centerbody. This is the beginning of the fifth shock cell for the baseline case and the sixth shock cell for the chevron case. For both configurations, the shock-cell spacing downstream of the centerbody tip slightly increases with secondary flow, which is well known and has been documented before [16–18]. The current results are showing this to be true when a centerbody is present and also when chevrons are used.

Table 1 presents the mean and rms of the normalized static pressure for all three cycle points and both nozzle configurations. Both statistical quantities were calculated over the first $5D_{\text{eq}}$. The mean is about the same for all cases, but the rms is slightly different, based on the cycle point. The secondary flow of $M_2 = 0.28$ is seen to have the highest rms, while $M_2$ of 0.00 and 0.50 have a much lower rms value. It will be shown in the far-field results that the Mach 0.28 jet had a strong screech tone, while the other two secondary flows had screech tones that were much much weaker compared with the Mach 0.28 flow. Finally, the table confirms that the chevron configuration does not significantly change the static pressure oscillations for any of the secondary flows. For the rest of the paper, the discussions will assume that the chevrons reduce the shock-cell length, but do not significantly reduce the shock-cell strength.

Figure 4 quantifies the shock-cell spacing for both the chevron and baseline configurations and compares it with the literature. The abscissa is the secondary-flow Mach number and the ordinate is the shock-cell spacing normalized by the jet diameter ($L/D_{\text{eq}}$). All cases have a positive slope, because the shock-cell spacing is increasing

**Table 1 Mean/rms of static pressure for measurements presented in Fig. 3**

| | $M_2 = 0.00$ | $M_2 = 0.28$ | $M_2 = 0.50$ |
|---|---|---|---|
| Baseline | 0.77/0.014 | 0.77/0.023 | 0.78/0.013 |
| Chevron | 0.77/0.016 | 0.76/0.021 | 0.77/0.016 |

with increasing secondary flow. The chevron cases have shorter shock-cell spacing, which is quantified by the downward shift of the line compared with the baseline case. When comparing with the literature, the Norum and Shearin [11] and Norum and Brown [21] cases were for a jet Mach number of 1.8 with design Mach number of 1.5; thus, the spacing should naturally be higher, but this is presented to support the increase in spacing with increased secondary flow. The Norum and Shearin [12] has the closest match to the current results, because their tests were with $M_j$ of 1.16, 1.22, and 1.28, while the current investigation has an $M_j$ of 1.19. Finally, with no secondary flow, the predicted normalized shock-cell spacing for a converging-only geometry at an $M_j$ of 1.19 is 0.71 (Harper-Bourne and Fisher [9]), while the current results have calculated a total spacing of 0.62. The most significant difference between the two configurations comes from the presence of a centerbody for the current configuration. Also, these empirical relations are for converging-only nozzles, and the current hardware geometry is more complex, as discussed in the experimental setup.

Radial turbulence intensity profiles at $X/D_{\text{eq}} = 2.0$ (left column) and $X/D_{\text{eq}} = 8.0$ (right column) for both configurations and all cycle points are shown in Fig. 5. The turbulence statistics are reported as a two-dimensional version of the turbulent kinetic energy (TKE):

$$\frac{\sqrt{\text{TKE}}}{V_{\text{exit}}} = \frac{\sqrt{\langle u^2 + v^2 \rangle}}{V_{\text{exit}}} \tag{1}$$

where $u$ is the axial and $v$ is the radial fluctuating velocity. For both configurations and at both axial positions, the inner-shear-layer turbulence intensity was a maximum when the secondary flow was set to Mach 0.00. This is seen by comparing the TKE values at $R/D_{\text{eq}} \sim 0.5$. As the secondary-flow Mach number was increased, the turbulence intensity in the inner shear layer decreased, due to a reduction in shear velocity. The reduction in shear velocity resulted in a slight increase in shock-cell spacing (see Fig. 4). The turbulence intensity in the outer shear layer was a minimum when the secondary flow was set to Mach 0.00 and increased as the secondary-flow velocity was increased. This is seen by comparing the TKE values at $R/D_{\text{eq}} \sim 1.125$.

Compared with the baseline case, the chevrons tend to increase the jet spread and thus reduce the gradients in the radial direction. The chevrons also raise the TKE levels at the upstream position ($X/D_{\text{eq}} = 2$) and reduce the TKE levels at the downstream position ($X/D_{\text{eq}} = 8$). The raised TKE levels and increased jet spread near the nozzle exit can be attributed to the streamwise vortices shed from the

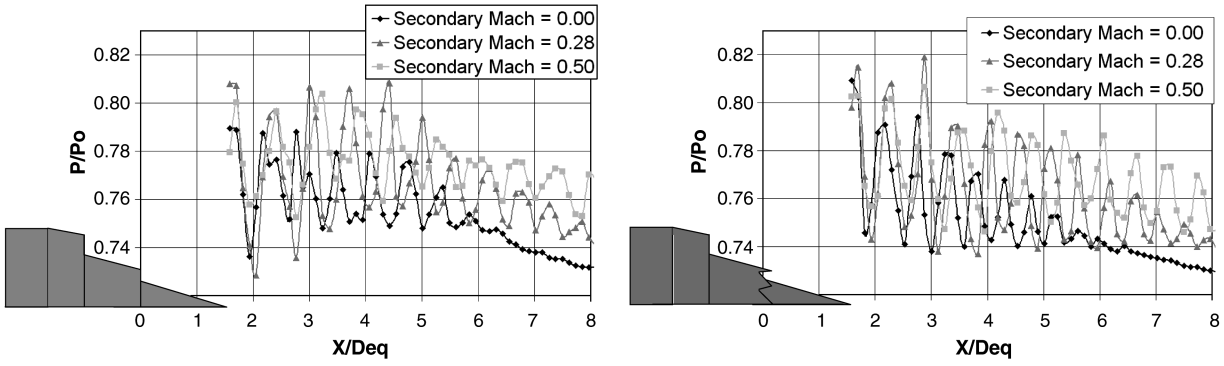


**Fig. 3 Normalized static pressure measurements for baseline and chevron configurations with variable-speed secondary flow.**

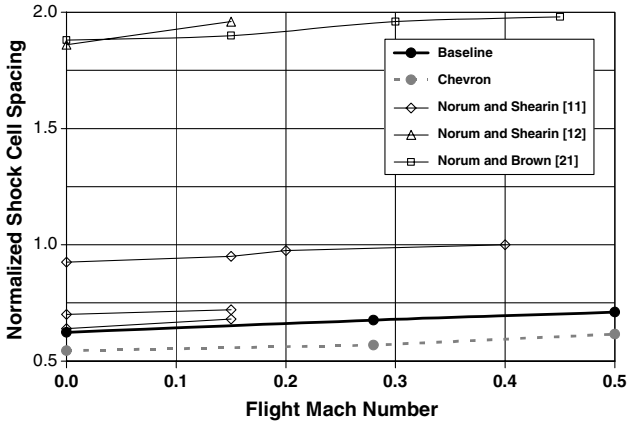


**Fig. 4 Normalized shock-cell separation ($L/D$) for baseline and chevron configurations at variable-speed secondary flow and comparison with various data.**

chevrons. Downstream, the streamwise vortices have broken down and the increased jet spread is accompanied by a reduction in the peak TKE values. This general trend is also seen in subsonic jets (Callender et al. [4]).

### B. Shock-Associated Noise

There are three significant changes to account for when making noise measurements and using a secondary stream to simulate forward-flight effects. The first is the secondary stream imposes convective effects. The second is the refraction effects due to the shear layer between the secondary stream and ambient air. The third effect is to account for the forward motion of the aircraft. The third effect is not accounted for in the current investigation, since an observer inside the cabin would be moving at the same speed as the aircraft. For the range of Mach numbers studied, the ray angle changes due to refraction and convection effectively cancel each other for the 70 deg measurement (Norum and Brown [21]). Changes due to refraction and convection at the aft angles for the mixing noise

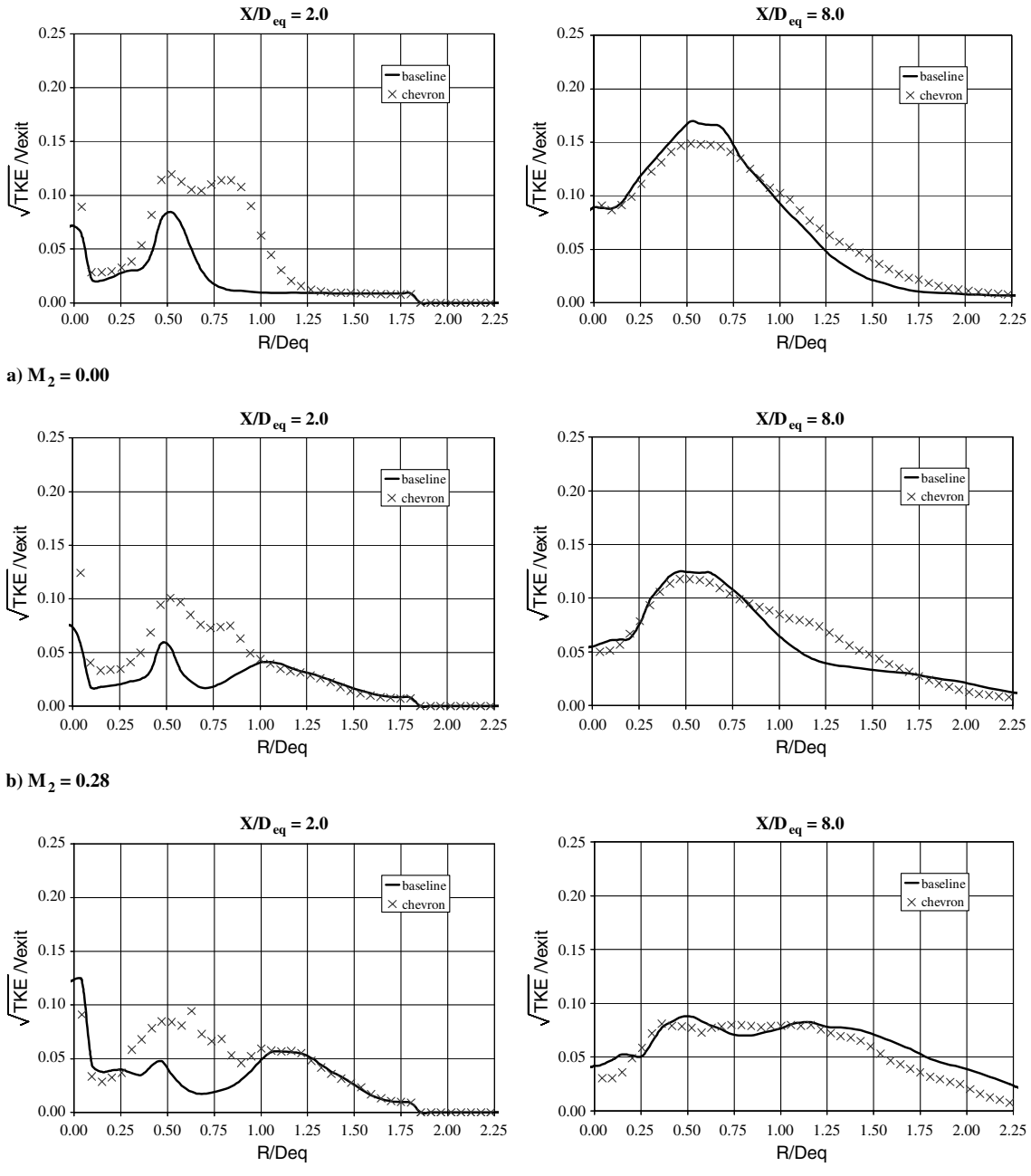


**Fig. 5 Flowfield results (TKE) at $X/D_{eq} = 2.0$ (left) and $X/D_{eq} = 8.0$ (right) for baseline and chevron configurations with secondary-flow Mach numbers of 0.0, 0.28, and 0.50.**

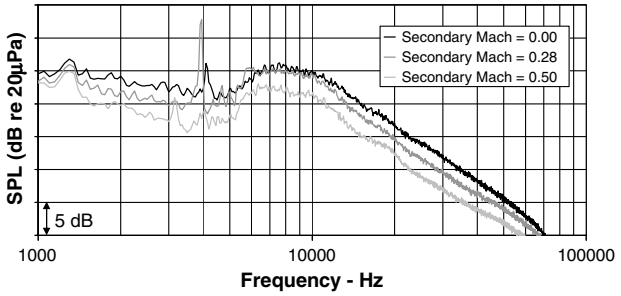


**Fig. 6 Far-field broadband shock-associated noise, 70 deg, primary flow = $M_j = 1.19$ with variable-speed secondary flow.**

requires presentation of observation angles equal to 150, 140, and 140 deg for $M_2$ of 0.00, 0.28, and 0.50, respectively [21].

Far-field shock-associated noise results for the baseline configuration at all cycle conditions are shown in Fig. 6. As a general trend, it can be seen that the center frequency of shock noise was slightly reduced with increasing secondary flow. The acoustic results suggest that the shock-cell spacing increased with increased secondary flow, which is consistent with the shock-cell spacing results presented in Fig. 4. As a second general trend, the magnitude of shock noise decreased when the secondary flow was increased from $M_2 = 0.00$ to 0.50. This result is consistent with the radial TKE profiles at $X/D_{\text{eq}} = 2.0$ shown in Fig. 5. The similarity between the TKE profile and the shock noise is because shock noise is generated as the turbulence interacts with the shocks cells. The decrease in frequency and reduction in amplitude for shock-associated noise with increasing secondary flow was also seen by Norum and Brown [21]. The one anomaly is the $M_2 = 0.28$ case, which has a slight increase in noise compared with the $M_2 = 0.00$ case around 7 kHz. This case has a screech tone and higher rms static pressure (refer back to Table 1), which ultimately leads to increased noise around 7 kHz. The turbulence measurements do not show this anomaly; instead, they monotonically decrease with increasing secondary Mach number. Thus, the screech tone looks to be identified through the static pressure rms and not changes in turbulence.

To study the chevron effect, far-field shock-associated noise results for both the baseline and chevron configurations and all cycle conditions are shown in Fig. 7. The results for different secondary Mach numbers have been offset for ease of viewing. As a first observation, note that the screech tones are much more significant with the baseline configuration. This is particularly true when the secondary flow was Mach 0.28. The chevron nozzle configuration works to attenuate the screech tones. Screech tones are created by a feedback loop [22]. Sound waves are created as the turbulent eddies pass through the shock cells. The sound waves then propagate upstream just outside of the supersonic flow and affect the turbulent eddies discharging from the nozzle. The loop is closed when the new eddies interact with the shock cells and generate more noise as they advect downstream. Chevrons alter the trailing edge of a nozzle and do not provide a reflecting surface that is normal to the flow like a baseline nozzle. This change in geometry may be responsible for

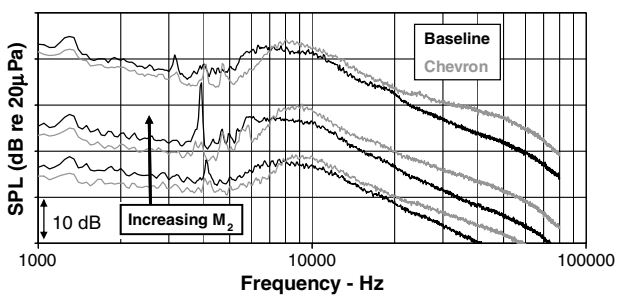


**Fig. 7 Comparison between baseline and chevron far-field broadband shock-associated noise, at an observation angle of 70 deg with variable-speed secondary flow.**

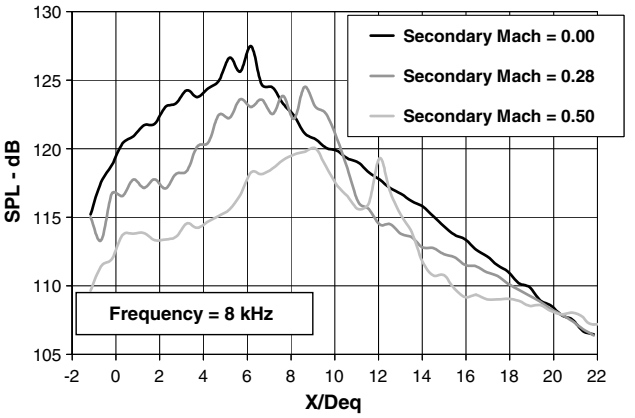


**Fig. 8 Near-field shock noise (SPL) at 8 kHz for baseline configuration for varying secondary-flow speed.**

disrupting the feedback loop and, as a result, reducing the screech tones.

As a second observation, the chevrons always increased the center frequency of shock noise. This increase in frequency is a result of the reduction in shock-cell spacing for the chevron configuration, as supported by the shadowgraph and static pressure measurements presented in Figs. 2–4, respectively. As a final observation from Fig. 7, note that chevrons increase shock noise. The TKE results at $X/D_{\text{eq}} = 2$ showed that the chevrons raised the turbulence levels in the shear layer between the core stream and secondary flow. It was also shown in Table 1 that the static pressure oscillations were similar between the baseline and chevron cases. Thus, the increase in shock noise can be attributed to the increase in turbulence and not to changes in the shock-cell strength.

Near-field pressure results at 8000 Hz for the baseline and all three secondary flows are shown in Fig. 8. Recall from Fig. 7 that this is a reasonable frequency for shock noise comparison. Shown for the baseline case (and also true for the chevron case, but not shown) is that the magnitude of shock noise dropped with increasing secondary flow and reached a minimum at Mach 0.50. This again can be attributed to the reduction in turbulence levels shown in Fig. 5. A second observation is that increasing the secondary flow tended to move shock noise generation farther downstream. The peak amplitude moving downstream is most consistent with the static pressure results. For $M_2 = 0.00$, the normalized static pressure oscillations have died out by $X/D_{\text{eq}} = 6$ (refer back to Fig. 3), which is the same location as the peak amplitude for broadband shock-associated noise in Fig. 8. For $M_2 = 0.28$, the normalized static pressure oscillations are almost gone by $X/D_{\text{eq}} = 8$, which is near the maximum for the broadband shock-associated noise. Finally, for $M_2 = 0.50$, the peak near-field pressure amplitude and the normalized static pressure oscillations persist the farthest downstream.

Figure 9 compares the baseline results to the chevron results at each secondary-flow Mach number. These data are at 10, 10, and 8 kHz for secondary flows of $M_2 = 0.00$, 0.28, and 0.50, respectively. Reference to the far-field acoustic results shown in Fig. 7 demonstrates that these are ideal frequencies for shock noise comparison. The chevrons increased the magnitude of shock noise and move the shock noise generation upstream. This is consistent with the decreased shock-cell spacing seen for the chevrons in Fig. 4. These results can be explained in much the same way as they were when considering a variable-speed secondary flow. The increased levels of upstream turbulence combined with similar static pressure fluctuations meant that chevrons increased the magnitude of shock noise.

### C. Trends in Mixing Noise

The far-field sound pressure level (SPL) and OASPL for the baseline configuration with secondary-flow Mach numbers of 0.00, 0.28, and 0.50 are shown in Fig. 10 and Table 2, respectively. To account for refraction and convection effects, observation angles of

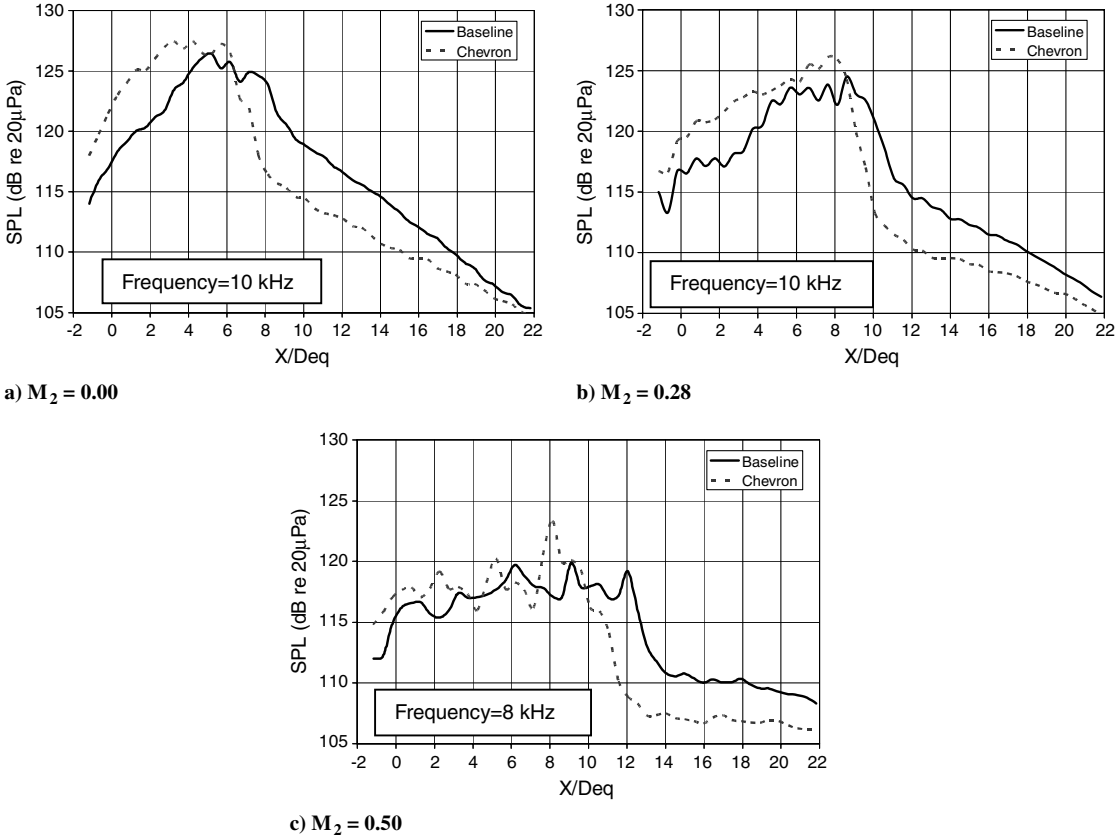


**Fig. 9 Comparison of near-field shock-associated noise between baseline and chevron configurations at various secondary-flow Mach numbers.**

150, 140, and 140 deg are presented for $M_2$ of 0.00, 0.28, and 0.50, respectively [21]. Turbulent mixing noise is the dominant component of jet noise at these angles. It is generated in the mixing region, which is defined as the region of high turbulence that results as the potential core velocity begins to decay. Results indicate that the highest noise levels occurred when $M_2$ was 0.00. The SPL and OASPL decreased when the secondary flow was increased to Mach 0.28 and then again for secondary-flow Mach number of 0.50.

This phenomenon was initially explained by Balsa [23], where *predicted* noise levels matched *measured* noise levels at different velocity (fan to core) and area (fan to core) ratios. It was explained that the "Noise minimum [was] a direct consequence of the reduction in turbulence intensity in the inner-to-outer stream mixing layer as the outer flow velocity [was] increased. Further increases in outer flow velocity cause[d] the outer-to-ambient stream mixing layer turbulence to produce the dominant noise." Similar results are seen in Fig. 10, and the turbulence levels at $X/D_{\text{eq}} = 8.0$ (Fig. 5) agree with the explanation of Balsa [23].

The specific value of simulated flight Mach number required for a noise minimum varies with the cycle condition and geometrical configuration of the tests. The noise minimum for the current configuration occurred between Mach 0.50 and Mach 0.85. Although not presented due to its inability to properly simulate flight effects, tests were run for a secondary-flow Mach number of 0.85. The OASPL for the Mach 0.85 case did have a 3 dB increase in OASPL compared with the Mach 0.50 case, due to the dominance of the outer shear layer, as discussed in Balsa [23].

Comparisons of the SPL and OASPL for both the baseline and chevron nozzles and all secondary-flow Mach numbers are shown in Fig. 11 and Table 2, respectively. Similar to Fig. 7, SPL for different secondary-flow velocities have been vertically offset to allow for easy and uncluttered viewing. In all cases, chevrons reduced the low-frequency mixing noise and OASPL. The effect of the chevrons was reduced as the secondary Mach number increased. These data demonstrate that the effect of chevrons decreases as the shear velocity decreases. The high-frequency penalty associated with the chevrons is most prevalent when the secondary-flow Mach number is 0.00. As the secondary-flow Mach number is increased this penalty goes away. The current conclusion shows that increasing the secondary flow has many similarities to decreasing the chevron penetration [2].

Near-field SPL results at a narrowband frequency of 1250 Hz for the baseline case and all secondary-flow Mach numbers are shown in Fig. 12. The same trend is evident for the near-field pressure, as was

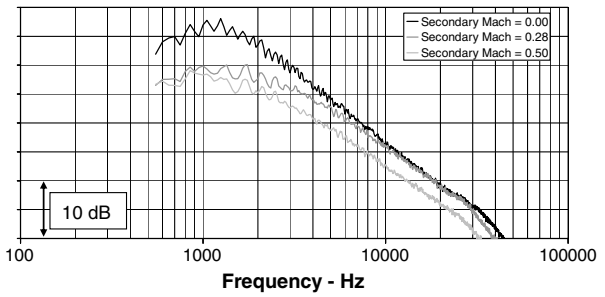


**Fig. 10 Far-field mixing noise for secondary-flow Mach numbers of 0.00, 0.28, and 0.50 and at angles of 150, 140, and 140 deg, respectively.**

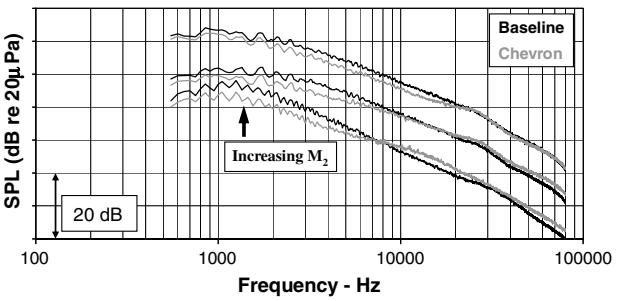


**Fig. 11 Far-field mixing-noise comparison between baseline and chevron configurations for variable-speed secondary-flow Mach numbers.**

**Table 2 OASPL for baseline and chevron core nozzles with varying secondary flow**

| | $M_2 = 0.00$ | $M_2 = 0.28$ | $M_2 = 0.50$ |
|---|---|---|---|
| Baseline | 117.4 | 112.9 | 111.2 |
| Chevron | 115.1 | 111.1 | 110.0 |

seen with the SPL: the mixing noise is reduced as $M_2$ increased from 0.00 to 0.50. The same trend was also seen for the chevron configu ration as $M_2$ was increased but not shown. Aside for the SPL reduction, the peak noise levels only move slightly downstream as $M_2$ increases, which is most likely due to the slight increase in potential core length as $M_2$ is increased.

Near-field acoustic results at 1250 Hz comparing the baseline and chevron configurations at all $M_2$ are shown in Fig. 13. The chevron nozzle reduces the low-frequency mixing noise in the near field and far field for all $M_2$. These results are very consistent with the turbulence measurements at $X/D_{eq} = 8.0$. The most significant turbulence reduction by the chevron was for $M_2 = 0.00$. This case has the highest shear velocity, allowing the chevron to generate the strongest streamwise vortices. The effect of the chevron was incrementally reduced with increasing $M_2$, which is again consistent with the turbulence measurements at $X/D_{eq} = 8.0$.

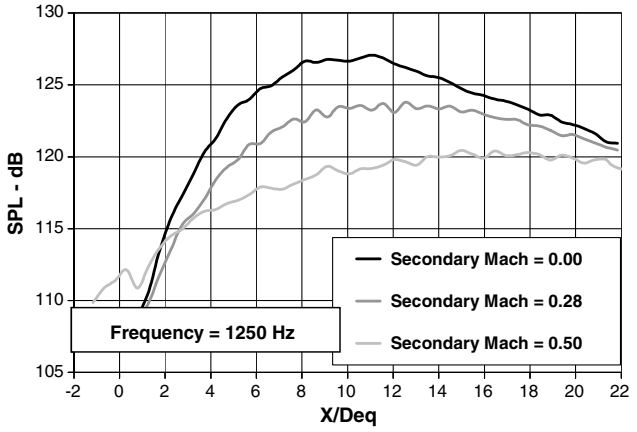


**Fig. 12 Near-field mixing noise (SPL) at 1250 Hz for baseline configuration with variable secondary flow.**

## IV. Conclusions

Tests were conducted to determine how chevrons affect the sound radiated from the exhaust of an underexpanded Mach 1.19 jet under simulated flight effects. A baseline nozzle and a chevron nozzle were tested on the core stream in a coaxial nozzle configuration. The secondary flow was varied from quiescent to Mach 0.50. Shadowgraphy, near-field static pressure, and turbulence measurements were used to complement near-field and far-field acoustic measurements.

Far-field measurements at 70 deg showed that the chevrons reduced any screech tones, increased the center frequency of shock-associated noise, and slightly increased the shock noise. Near-field pressure measurements showed that the chevrons shifted the peak location for shock noise generation upstream. Static pressure measurements demonstrated that chevrons always decreased the shock-cell spacing, which explained the increase in frequency for the acoustic results and upstream movement of the shock noise generation. The chevrons had increased turbulence levels near the nozzle exit ($X/D_{eq} = 2$), and the chevrons had almost no effect on static pressure spatial fluctuations (see Table 1). The chevrons having higher turbulence levels and similar static pressure fluctuations compared with the baseline seems to support that the increased turbulence levels were responsible for the higher peak amplitude of the shock-associated noise for the chevron case.

While the results nicely demonstrated the mechanisms behind the change in shock-associated noise when the chevrons are used, it would be ideal to see a reduction in shock-associated noise.

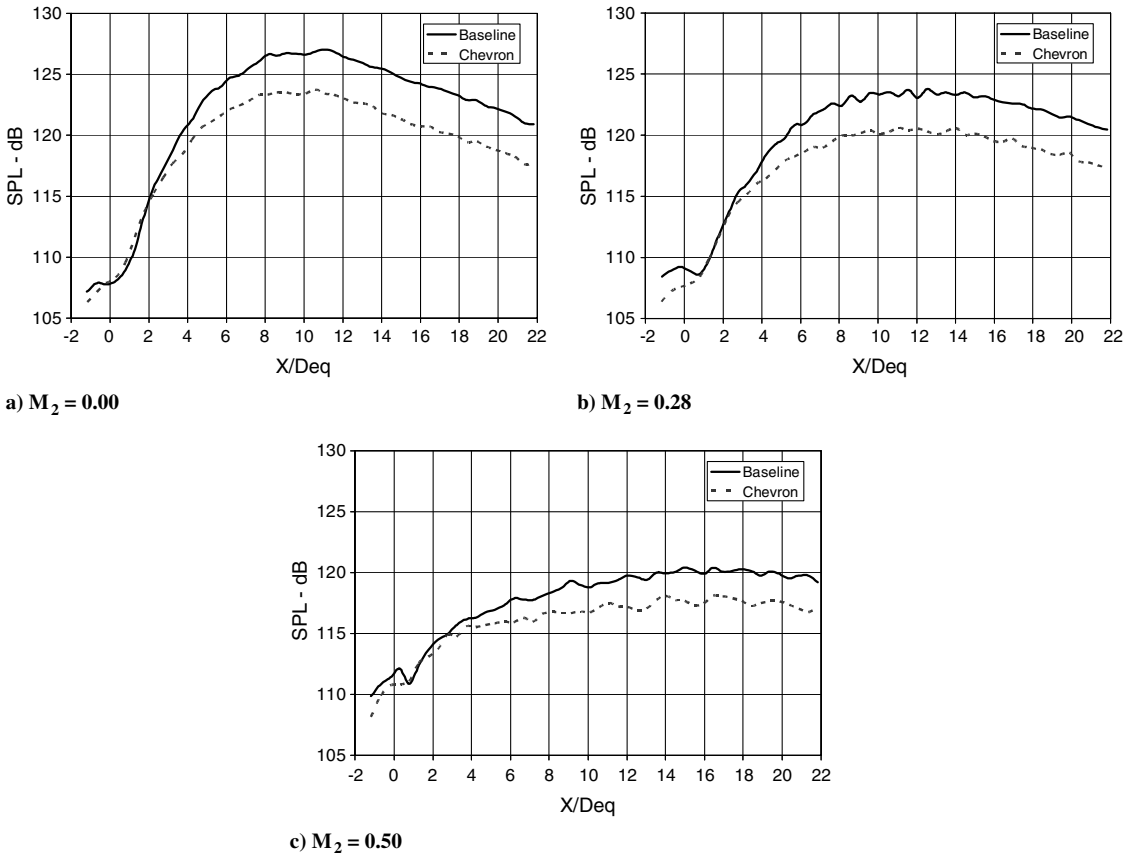


**Fig. 13 Comparison of near-field mixing noise at 1250 Hz between baseline and chevron configurations at various secondary-flow Mach numbers.**

However, only one chevron penetration case was studied and the number of chevrons was fixed at eight. Callender et al. [2] suggested that due to the number of different cycles and shear velocities on modern turbofan engines, the optimum chevron penetration/number probably varies from engine to engine. Shock noise is particularly sensitive to variations in the cycle point and is likely to be just as sensitive to chevron design. Therefore, optimum chevron design for broadband shock noise reduction must probably be tailored to particular engines and engine cycles. This was also suggested by Long [15].

Far-field measurements at the aft angles demonstrated that increasing secondary flow reduced the mixing noise. This was documented for both baseline and chevron configurations. Flowfield results showed that the inner shear layer had the highest TKE values at the downstream position ($X/D_{\text{eq}} = 8$) for low secondary flows. As the secondary flow was increased, the inner shear layer grew weaker and the mixing noise and downstream turbulence levels were consequently reduced. The chevrons always reduced the mixing noise regardless of the secondary-flow Mach number. This was again explained through reduced turbulence levels near the end of the potential core ($X/D_{\text{eq}} = 8$) when comparing the chevron case with the baseline case.

## References


[1] Saiyed, N., Mikkelsen, K., and Bridges, J., "Acoustics and Thrust of Separate-Flow Exhaust Nozzles with Mixing Devices for High Bypass-Ratio Engines," *AIAA Journal*, Vol. 41, No. 3, 2003, pp. 372–378. doi:10.2514/2.1986

[2] Callender, W. B., Gutmark, E., and Martens, S., "Far-Field Acoustic Investigation into Chevron Nozzle Mechanisms and Trends," *AIAA Journal*, Vol. 43, No. 1, 2005, pp. 87–95. doi:10.2514/1.6150

[3] Callender, W. B., Gutmark, E., and Martens, S., "Near-Field Investigation of Chevron Nozzle Mechanisms," *AIAA Journal*, Vol. 46, No. 1, 2008, pp. 36–45. doi:10.2514/1.17720

[4] Callender, W. B., Gutmark, E., and Martens, S., "A PIV Flow Field Investigation of Chevron Nozzle Mechanisms," AIAA Paper 2004-0191, 2004.

[5] Rask, O., Gutmark, E., and Martens, S., "Acoustic Investigation of a High Bypass Ratio Separate Flow Exhaust System with Chevrons," AIAA Paper 2004-0009, 2004.

[6] Rask, O., Gutmark, E., and Martens, S., "Near Field Acoustics of Core and Fan Chevrons Nozzles," AIAA Paper 2007-0436, 2007.

[7] Rask, O., Gutmark, E., and Martens, S., "A PIV Flow Investigation of Medium Bypass Chevron Nozzles," AIAA Paper 2007-0436, 2007.

[8] Herkes, W., Olsen, R., and Uellenberg, S., "The Quiet Technology Demonstrator Program: Flight Validation of Airplane Noise-Reduction Concepts," AIAA Paper 2006-2720, 2006.

[9] Harper-Bourne, M., and Fisher, M. J., "The Noise from Shockwaves in Supersonic Jets," *Proceedings of the AGARD Conference on Noise Mechanisms*, AGARD CP-131, Neuilly-sur-Seine, France, 1973.

[10] Norum, T. D., and Seiner, J. M., "Measurements of Static Pressure and Far Field Acoustics of Shock Containing Supersonic Jets," NASA TM 84521, 1982.

[11] Norum, T. D., and Shearin, J. G., "Effects of Simulated Flight on the Structure and Noise of an Underexpanded Jet," NASA TP-2308, 1984.

[12] Norum, T. D., and Shearin, J. G., "Shock Structure and Noise of Supersonic Jets in Simulated Flight to Mach 0.4," NASA TP-2785, 1988.

[13] Samimy, M., Zaman, K. B. M., and Reeder, M. F., "Effect of Tabs on the Flow and Noise Field of an Axisymmetric Jet," *AIAA Journal*, Vol. 31, No. 4, 1993, pp. 609–619. doi:10.2514/3.11594

[14] Long, D. F., "The Structure of Shock Cell Noise from Supersonic Jets," AIAA Paper 2005-2840, 2005.

[15] Long, D. F., "Effect of Nozzle Geometry on Turbofan Shock Cell Noise at Cruise," AIAA Paper 2005-0998, 2005.

[16] Mengle, V., Ganz, U., Nesbitt, E., and Bultemeier, E., "Flight Test Results for Uniquely Tailored Propulsion-Airframe Aeroacoustic Chevrons: Shockcell Noise," AIAA Paper 2006-2439, 2006.

[17] Bultemeier, E. J., Ganz, U., Premo, J., and Nesbitt, E., "Effect of Uniform Chevrons on Cruise Shockcell Noise," 27th AIAA Aeroacoustics Conference, AIAA Paper 2006-2440, May 2006.

[18] Callender, W. B., Gutmark, E., and Dimicco, R., "The Design and Validation of a Coaxial Nozzle Acoustic Test Facility," AIAA Paper 2002-369, 2002.

[19] Melling, A., "Tracer Particles and Seeding or Particle Image Velocimetry," *Measurement Science and Technology*, Vol. 8, No. 12, 1997, pp. 1406–1416. doi:10.1088/0957-0233/8/12/005

[20] Cooper, M., and Webster, R., "The Use of an Uncalibrated Cone for Determination of Flow Angles and Mach Numbers at Supersonic Speeds," NASA/NACA TN-2190, 1951.

[21] Norum, T. D., and Brown, M. C., "Simulated High Speed Flight Effects on Supersonic Jet Noise," AIAA Paper 93-4388, 1993.

[22] Powell, A., "On the Mechanism of Choked Jet Noise," *Proceedings of the Physical Society of London*, Sect. B66, Taylor and Francis, London, pp. 1039–1057.

[23] Balsa, T. F., "The Far Field of High Frequency Convected Singularities in Sheared Flows, with an Application to Jet-Noise Prediction," *Journal of Fluid Mechanics*, Vol. 74, No. 2, March 1976, pp. 193–208. doi:10.1017/S0022112076001766


C. Bailly
*Associate Editor*